

# Nonadiabatic Molecular Dynamics Study of the Relaxation Pathways of Photoexcited Cyclooctatetraene

Huajing Song,\* Yeonsig Nam, Daniel Keefer, Marco Garavelli, Shaul Mukamel, and Sergei Tretiak\*



Cite This: *J. Phys. Chem. Lett.* 2021, 12, 5716–5722



Read Online

ACCESS |



Metrics & More

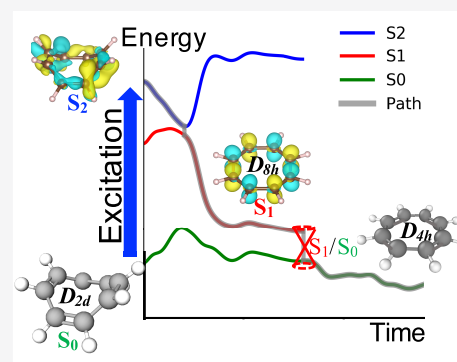


Article Recommendations



Supporting Information

**ABSTRACT:** In the current study, we present nonadiabatic (NAMD) and adiabatic molecular dynamics simulations of the transition-state dynamics of photoexcited cyclooctatetraene (COT). The equilibrium-state structure and absorption spectra are analyzed using the semiempirical Austin Model 1 potential. The NAMD simulations are obtained by a surface-hopping algorithm. We analyzed in detail an active excited to ground state relaxation pathway accompanied by an  $S_2/S_3(D_{2d}) \rightarrow S_1(D_{8h}) \rightarrow S_0(D_{4h}) \rightarrow S_0(D_{2d})$  double-bond shifting mechanism. The simulated excitation lifetime is in good agreement with experiment. The first excited singlet state  $S_1$  plays a crucial role in the photochemistry. The obtained critical molecular conformations, energy barrier, and transition-state lifetime results will provide a basis for further investigations of the bond-order inversion and photoswitching process of COT.



Photoswitches are molecular systems that change their geometry and properties upon optical excitation<sup>1,2</sup> and may find applications in biology, chemistry, and nanotechnology. Photoisomerization is a typical example of such switching,<sup>3–5</sup> for example, observed in rhodopsin, which constitutes an initial step in human and animal vision.<sup>6,7</sup> Cyclooctatetraene (COT) is a conjugated cyclic  $4n$   $\pi$ -electron system that gains aromaticity with a planar structure with equal C–C bond lengths in the first singlet excited state  $S_1$  but is nonaromatic in higher excited states  $S_{n>1}$  and in the ground state ( $S_0$ ), where it assumes a nonplanar boat-like structure with localized single and double C–C bonds. Upon UV excitation, COT's nonradiative decay via a polyradical  $S_1/S_0$  conical intersection also promotes a bond-order inversion in the ground state, which is also known as double-bond shift (i.e., a  $\pi$ -skeletal rearrangement).<sup>8</sup> This process occurs when the  $\pi$ -electrons “migrate” within the octagonal perimeter resulting in a site exchange between singly and doubly bonded carbon atoms. Such a photoinduced double-bond shifting reaction may be exploited to design photochemically driven molecular switches,<sup>1</sup> where an “on-state” is characterized by a “through-conjugation” between the  $\pi$ -donor and  $\pi$ -acceptor substituents, whereas an “off-state” refers to a suppression of this through-conjugation. COT thus appears as a particularly suitable candidate for studying both the double-bond shifting and the nonaromatic ( $S_0$ )/aromatic ( $S_1$ ) photoswitching process.<sup>8–11</sup>

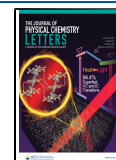
The excited-state relaxation pathway plays a key role in its photochemistry. Using complete active space self-consistent field (CASSCF) and CAS second-order perturbation theory (CASPT2) with the minimum energy path (MEP) method, Garavelli et al.<sup>8</sup> have identified some possible pathways for the

formation of photochemical structures of COT. A proposed mechanism describes that the photon initially excites COT to the bright (i.e., optically allowed)  $S_2$  state, which decays then efficiently to the dark (i.e., optically forbidden)  $S_1$  state. The following nonadiabatic transitions the ground state  $S_0$  appear to be controlled by two different tetradical-type conical intersections, which are accessed by  $S_1$  excited-state reaction paths. The higher-energy conical intersection configuration ( $CI_{st}$ ) is featured by a triangular  $-(CH)_3-$  kink, and the lowest-energy conical intersection has a folded quasi-tetradical structure  $CI_b$ . Further relaxation on the  $S_0$  potential-energy surfaces results in different product channels. In a series of recent studies, Takayanagi et al.<sup>10,12,13</sup> have applied the ground-state ab initio molecular dynamics (MD) to study the photoionization of COT. However, because of the lack of appropriate excited-state potential and conical intersection dynamics information, the time scale obtained from their reduced-dimensionality quantum dynamics calculations and the on-the-fly classical dynamics calculations is too short compared to the experiment. By thermal fluctuations, only one (or two) relaxation pathways would dominate the excited-state dynamics at finite temperatures. Here we apply a nonadiabatic molecular dynamic (NAMD) simulation method to study the

Received: April 29, 2021

Accepted: June 9, 2021

Published: June 15, 2021



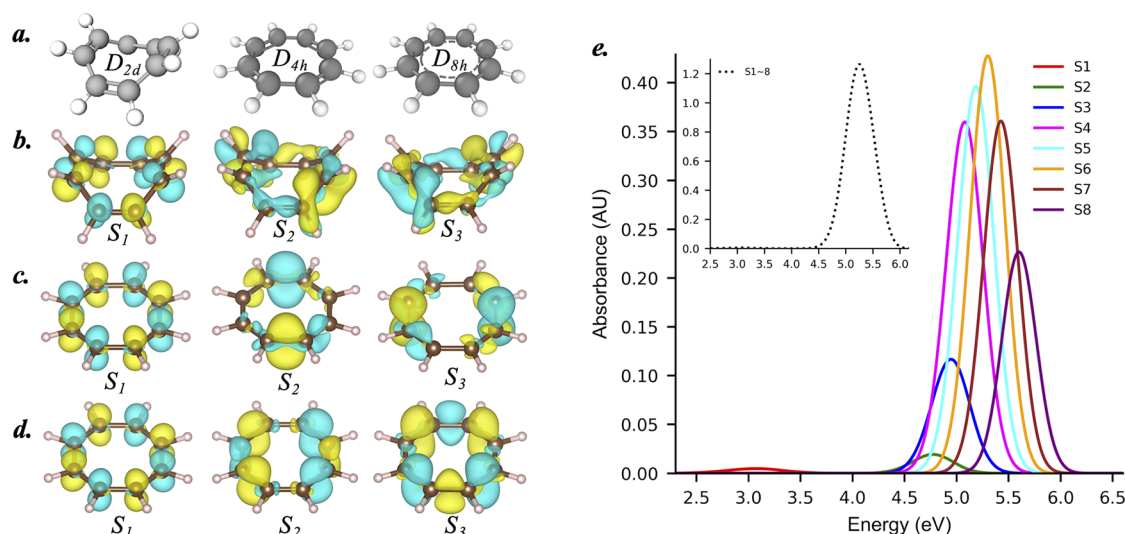


**Figure 1.** (a) Ground-state minimum geometry  $D_{2d}$  with bond lengths 1.344 Å (C=C) and 1.479 Å (C–C). Ground-state transition (meta-stable) geometry  $D_{4h}$  with bond lengths 1.336 Å (C=C) and 1.442 Å (C–C). Native optimal  $S_1$  geometry  $D_{8h}$  with equal C–C bond lengths of  $\sim 1.387$ – $1.382$  Å. (b) Orbital plots of the TD for the lowest three electronic states at the ground-state optimized geometry. (c) The same but for the ground-state transition geometry. (d) The same but for the optimal  $S_1$  geometry. (e) Calculated absorption spectrum of COT at 300 K showing individual contributions of the eight lowest excited electronic states. (inset) The total absorption profile combining  $S_1$  to  $S_8$  contributions.

excited-state dynamics and determine the relaxation pathways of photoexcited COT.

The excited-state molecular dynamics of COT is calculated using Tully's fewest switches surface hopping (FSSH)<sup>14</sup> approach combined with empirical decoherence corrections<sup>15</sup> and trivial crossing tracking<sup>16</sup> algorithms as implemented into the Nonadiabatic Excited-state Molecular Dynamics (NEXMD) package.<sup>17–19</sup> By applying the collective electron oscillator method<sup>20</sup> with the semiempirical Austin Model 1 (AM1) Hamiltonian<sup>21</sup> at the configuration interaction singles (CIS)<sup>22</sup> level, the NEXMD can routinely handle the NAMD simulation up to 20 picoseconds (ps). This package has been successfully applied to the modeling of photoinduced processes in many other molecular systems.<sup>23–25</sup>

Our simulations find that COT has nonaromatic equilibrium boat-shaped structures in the ground state and higher excited states  $S_n$  ( $n = 2$  or  $3$ ) and planar antiaromatic metastable structures in the ground state. The equilibrium structure in  $S_1$  is aromatic (Figure 1a). The transition between the three aromaticities may be induced either thermally or photochemically.<sup>9,26,27</sup> A geometric optimization was performed by starting with a boat-shaped or planar structure in all  $S_0$  to  $S_3$  states. We were unable to optimize the structure of COT ( $S_2$ ) due to the small band gap with  $S_1$  pointing to the lack of a well-defined potential-energy minimum (as detailed in the Supporting Information). As shown in Figure 1a, both of the  $D_{2d}$  symmetric boat-shaped minimum nonaromatic structures and the planar  $D_{4h}$  symmetric transition antiaromatic structures can be obtained by a geometric optimization in  $S_0$ , with a slightly higher potential energy ( $\Delta E = 0.5$  eV) for the planar  $D_{4h}$  structure. The significant variances between the single- and double-bond lengths (listed in the Figure 1 caption and refs 28 and 29) identified their aromaticity. For comparison, the native minimum  $S_1$  structure has an aromaticity with  $D_{8h}$  symmetry due to its planar geometry and a vanishing C–C bond length difference (0.005 Å). The band gaps are then analyzed based on the true boat-shaped  $S_0$  optimal structure. Table 1 compares the vertical excitation energies calculated by different

**Table 1. Comparison of the Vertical Excitation Energies (in eV) for the First Three Singlet Excited States of COT for Different Methods<sup>a</sup>**

method	$S_1$	$S_2$	$S_3$
AM1/CIS	3.06	4.95	4.97
TD-DFT	3.61	5.34	5.35
CASSCF <sup>8</sup>	6.26	7.01	6.54
CASPT2 <sup>8</sup>	4.00	5.75	6.00

<sup>a</sup>TD-DFT simulations were performed with PBE0 functional and 6-31G\* basis set.

methods. As with other systems, the semiempirical AM1/CIS results in red-shifted energies compared to time-dependent density functional theory (TD-DFT) and ab initio CASSCF/CASPT2 methods. Importantly, the relaxation rates during the excited-state dynamics are closely related to the energy gaps between states<sup>25</sup> but not to the absolute values of the transition energies from the ground state. Therefore, the AM1/CIS approach is appropriate to conduct the COT NAMD simulation due to the good agreement of band gaps with other higher-level methods (e.g., TD-DFT and CASPT2).

Figure 1b shows the state transition density (TD) plotted for the first three singlet excited states of COT evaluated at the boat-shape  $S_0$  optimal geometry. The TD of  $S_1$  state is evenly distributed at each C atom, while these quantities for  $S_2$  and  $S_3$  are disorderly distributed around the nonplanar ring. Figure 1c shows the same excited-state TDs, based on the  $S_0$  transition geometry. In the antiaromatic planar geometry, all three lowest electronic states exhibited an even TD distribution based on its symmetry around the ring. The antisymmetric structure of  $S_2$  and  $S_3$  TDs with respect to the horizontal and vertical planes, respectively, is pronounced. For comparison, the TDs of the  $S_1$  aromatic planar structure are also shown in Figure 1c. The  $D_{8h}$  COT has a pair of half-filled and degenerate nonbonding  $\pi$ -orbitals<sup>28</sup> (i.e., delocalized  $\pi$ -bond), in which the electrons freely move around the ring, as reflected by a broader  $S_2$  and  $S_3$  TD distribution in  $D_{8h}$  than in  $D_{4h}$ .

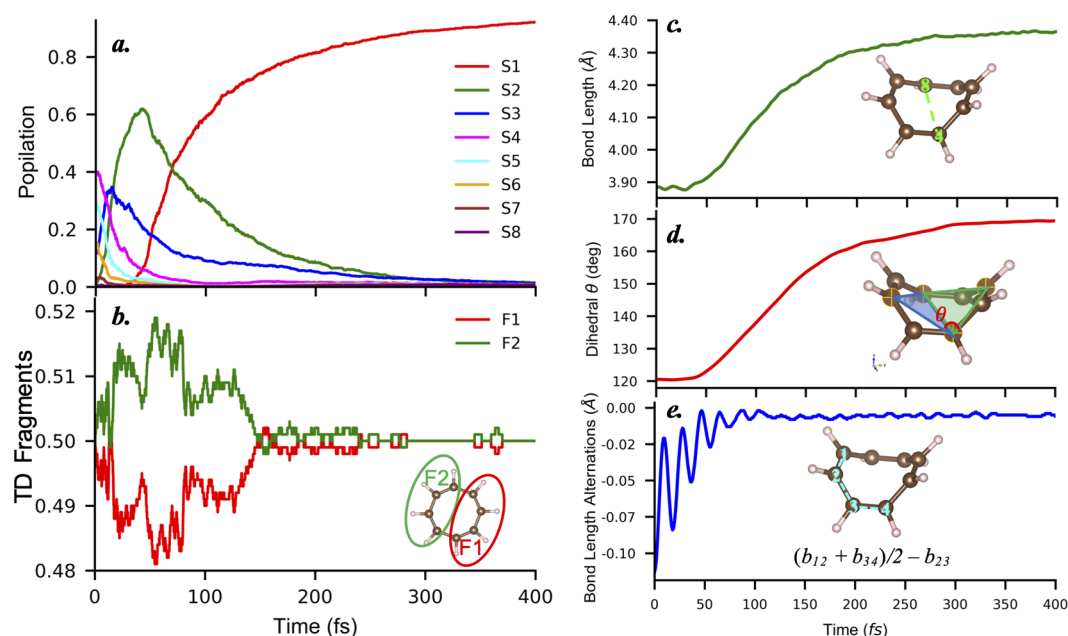


**Figure 2.** (a) Average populations of  $S_1$ – $S_8$  electronic states as a function of time from NAMD simulations. (b) Electronic transition density localized on each molecular fragment averaged over all trajectories. (c) Plot of the bond length  $b_{48}$  versus time. (d) Plot of the dihedral angle  $\theta$  over time. (e) Plot of the bond length alternations  $(b_{12} + b_{34})/2 - b_{23}$  over time.

To perform the NAMD simulations, we first conducted a sampling of the initial conformational structures by running a 520 ps ground-state adiabatic molecular dynamics (AMD) trajectory of COT in a vacuum using a Langevin thermostat at 300 K with a time step of 0.1 fs. Following a 20 ps equilibration period, 1000 snapshots of geometries and velocities were sampled every 0.5 ps as the initial conditions. The absorption spectrum analysis was performed on those initial samples with a Gaussian line shape and full width at half-maximum (fwhm) of 0.36 eV. The spectrum, shown in Figure 1e, includes the contributions of the eight lowest-energy excited states. The weakly absorbing  $S_1$  feature (a tiny peak at 3.1 eV) reflects a forbidden  $S_0$  to  $S_1$  excitation (dark state). The higher-energy states  $S_2$ – $S_8$  are optically bright transitions forming a strong absorption band between 5.0 and 5.8 eV. These results are in a good agreement with early COT measurements in a dye laser solution, which indicated an extremely weak absorption near 4.43 eV and an intense spectrum at 5.5–6.9 eV.<sup>30,31</sup>

The initial excited states were populated according to a Franck–Condon window  $g_i(r, R) = f_i \exp[-T^2(E_{\text{laser}} - E_i)^2]$ , where  $f_i$  and  $E_i$  are the oscillator strength and energy of excited state  $i$ , and  $E_{\text{laser}}$  is the energy of a Gaussian laser pulse  $f(t) = \exp(-t^2/2T^2)$ , centered at 5.0 eV, that corresponds to the maximum of the absorption for the  $S_4$  state (see Figure 1e), with a  $T = 0.36$  eV fwhm. The excited-state dynamics were then investigated using surface-hopping NAMD in vacuum at 300 K with a nuclear time step of 0.025 fs and an electron time step of 0.005 fs (see our previous NEXMD applications for more detail<sup>17–19</sup>). Eight excited states were included in the simulations to allow for possible transitions to higher energy. The instantaneous decoherence correction and trivial un-avoided crossings tracking were activated.

During NAMD, the overall nonradiative relaxation across a trajectory ensemble can be monitored by tracking the evolution of the averaged adiabatic state populations, TD profile, and COT geometry features. Figure 2a shows the quantum-state populations<sup>19</sup> in an NAMD simulation.

According to the Franck–Condon window with a 5.0 eV light impulse, the initially excited electronic states were concentrated around the  $S_3$ – $S_6$  band of states. Approximately 50% of the trajectories relaxed back to  $S_1$  in 100 fs. After 400 fs, 90% of the trajectories have arrived in  $S_1$ . To monitor the spatial energy transfer, the averaged time-dependent localization of the electronic TD among different fractions<sup>19</sup> of the COT molecule was tracked across the 1000 trajectories in total as depicted in Figure 2b. The transition density is evenly separated into two fractions (see the inset of Figure 2b) on the ring, in which fragment F2 collected the TD contributions from C atoms 1, 2, 3, 4, and their bonding H atoms (refer to the inset in Figure 2e), and fragment F1 is the sum of the TD from the rest of the carbon atoms. Finally, Figure 2c–e plots the relevant geometric features (bond length, dihedral angle, and bond length alternation) monitoring the geometry evolution of COT in the NAMD process. The selection of these parameters is detailed in the Supporting Information.

As indicated by Garavelli et al.,<sup>8,9</sup> the photoinduced double-bond shifting mechanism included a transfer of localized  $\pi$ -bonds to form a delocalized aromatic  $\pi$ -system (Figure 2a) during the  $D_{2d}$  to  $D_{8h}$  structure transformation. A similar process is observed in our SH-NAMD simulations. As shown in Figure 2b,c, the  $D_{2d}$  structure has an uneven TD distribution in the  $S_{n>1}$  states and a uniform TD distribution in  $S_1$ . Therefore, the strong TD fluctuation between the F1 and F2 segments in the initial 150 fs of dynamics in Figure 2b reflects an energy redistribution due to the fundamental  $\pi$ -bond transformation underpinning the double-bond shift. Meanwhile, the significant bond-length oscillation shown in Figure 2e was observed in the first 100 fs. Such oscillations in photoexcited molecular dynamics frequently signify the appearance of coherent electronic-vibrational dynamics persisting across an ensemble of trajectories.<sup>32</sup> Finally, when the molecule relaxes to a  $D_{8h}$  aromatic structure ( $S_1$ ), the localized  $\pi$ -bonds overlap to form a delocalized aromatic  $\pi$ -system across all C atoms of the ring. This explains the uniform TD



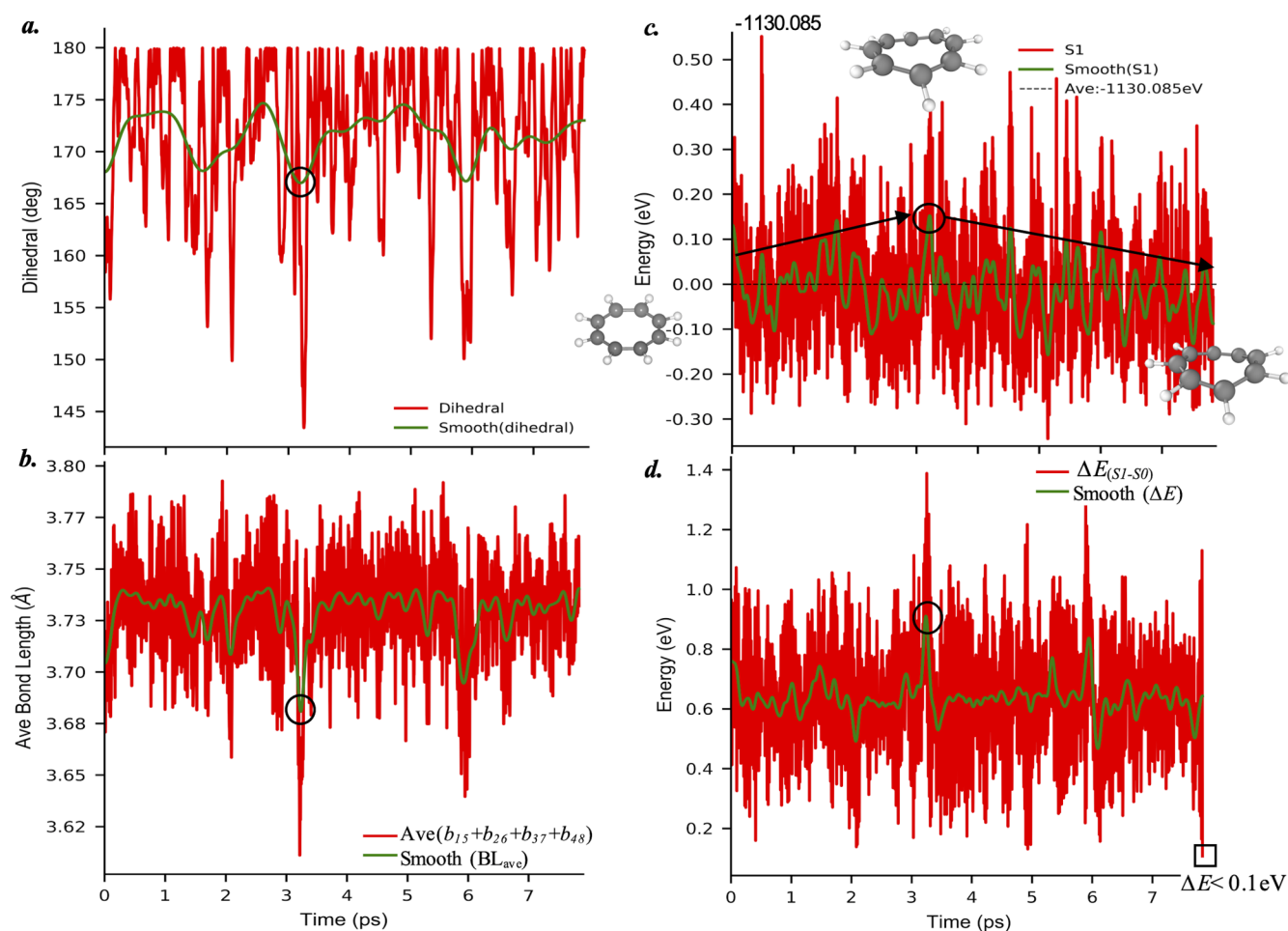


**Figure 3.** Analysis of a typical AMD trajectory on the  $S_1$  state. Plots of the dihedral angle (a), the average bond lengths ( $b_{15}$ ,  $b_{48}$ ,  $b_{37}$ , and  $b_{48}$ ) between all diagonal atoms (b), the total  $S_1$  state energy referenced with respect to its average  $-1130.085$  eV (c), and the  $\Delta E_{S_0-1}$  energy gap (d) with time. The green line in each plot is an average using the Savitzky-Golay filter<sup>43</sup> for every 100 data points.

distribution across fragments and diminishing bond length alternation when most of the trajectories were transferred to  $S_1$  after 150 fs.

Internal conversion in molecular systems across a manifold of excited electronic states occurs on ultrafast time scales, typically below  $\sim 1$  ps.<sup>33</sup> In contrast, because of a large energy gap, nonradiative transitions back to the ground state usually happen on much longer (tens of picoseconds to nanosecond) time scales. Here, barrierless ultrafast photoisomerizations such as rhodopsin dynamics<sup>7</sup> are notable exceptions. Descriptions of non-Born–Oppenheimer transitions to the ground state have an inherent multireference character and cannot be properly described with a single-reference method such as Hartree–Fock or density functional theory (DFT). For example, as mentioned in other published works,<sup>34,35</sup> conical intersections between the ground and excited states in the latter methods have an incorrect dimensionality owing to the Brillouin theorem.<sup>36,37</sup> This calls for the use of alternative approaches.<sup>22,38</sup> In a previous study,<sup>39</sup> we introduce a simple “Open-GS” method<sup>33,40</sup> to treat such transitions to the ground state: when the system is in the lowest-energy excited state and the energy gap between the ground and excited states ( $\Delta E_{S_0-1}$ ) is smaller than a certain threshold (normal 0.5 eV), the nonadiabatic transition is enforced, and the dynamics continues on the ground-state potential energy surface

(PES). Indeed, the  $\Delta E_{S_0-1}$  energy gap is becoming small in the COT molecule (see the Supporting Information) once the trajectory approaches the  $S_1/S_0$  conical intersection seam. We set a threshold  $\Delta E_{S_0-1} = 0.1$  eV to enforce the transition from the  $S_1$  to the  $S_0$  state with an excess of electronic energy redistributed into nuclear kinetic energy.<sup>41,42</sup> Accordingly, to model the final phase of COT photoinduced dynamics (i.e.,  $S_1/S_0$  transition), we selected 300 configurations from NAMD, which have stabilized in the  $S_1$  state for 10 fs without hopping upward to  $S_2$  as the initial conditions for the AMD simulation in the  $S_1$  state at 300 K. As this dynamics progressed, 291 terminated trajectories (out of 300 total) reached the  $S_1/S_0$  conical intersection seam within 20 ps of the  $S_1$  AMD. These trajectories were then reinitiated at the  $S_0$  state.

Figure 3a–d plots the geometric features and energy profile for a typical trajectory in an  $S_1$  AMD simulation. The trajectory sampling on the  $S_1$  PES in Figure 3c indicates that it traverses an energy barrier ( $\sim 0.3$  eV) before reaching the  $S_1/S_0$  conical intersection. When the barrier at 3.2 ps is crossed, a slight folding of the  $D_{8h}$  planar structure is detected, which is reflected as the valleys in the dihedral angle and average bond length plot (Figure 3a,b). By combining the geometric features with the  $\Delta E_{S_0-1}$  energy gaps shown in Figure 3d, we conclude that the folding deformation of the planar structure is accompanied by an increase of the  $\Delta E_{S_0-1}$  observed near the

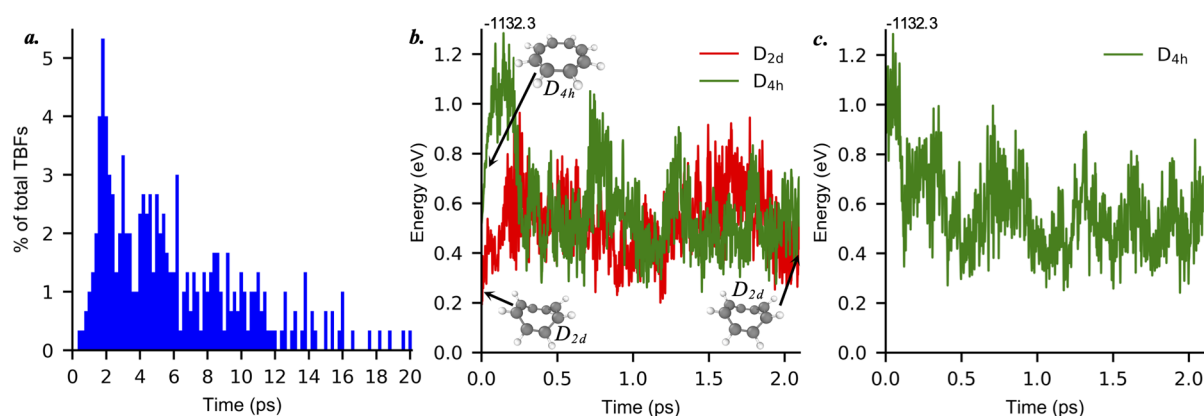


**Figure 4.** (a) Distribution of time scales for photoexcited COT before reaching  $S_1/S_0$  conical intersection. (b, c) Analysis of representative  $S_0$  AMD trajectories started from different conditions at 300 K. (b) Two trajectories initiated from  $D_{2d}$  boat-shape and planar  $D_{4h}$  COT structures. (insets) Initial and final COT geometries. (c) Trajectory initiated from the  $S_1/S_0$  transition structure. (b, c) Plots are referenced to the ground-state potential energy minimum  $-1132.3$  eV.

barrier (3.2 and 6 ps points). The results clearly show that, after crossing the energy barrier, the folded  $S_1$  structure needs to convert back to a less-folded conformation to be able to reach the  $S_1/S_0$  conical intersection. Compared to ref 8, the “planar-like” CI structure observed in our AMD simulations is somewhere between previously suggested folded (quasi-tetradical,  $CI_b$ ) and (triangular  $-(CH)_3$ - kink as  $CI_{st}$ ). We believe that such intermediate structures appear due to thermal effects in AMD, where trajectories reach the extended  $S_1/S_0$  crossing seam at different conical intersection conformations, eventually producing crossing points with intermediate structures with respect to the two extreme points located by the minimized energy paths presented in ref 8. Finally, the  $S_1$  AMD simulation is terminated once the  $\Delta E_{S_0-1}$  gets below 0.1 eV (Figure 3d).

Similar energy barrier crossing features were observed in all  $S_1$  AMD simulations; however, the  $S_1$  AMD trajectory lengths varied significantly. Compared to the  $S_{n>1}$  to  $S_1$  relaxation occurring within  $\sim 400$  fs, the  $S_1$  to  $S_0$  transition appears between 1 and 12 ps. In some extreme cases ( $<10\%$ ), the trajectory can stay on  $S_1$  for over 20 ps. Figure 4a shows the total excitation lifetime distribution of  $S_1$ . The peaks at  $\sim 1.6$  ps of the histogram plot indicated the possible excitation lifetime of COT before reaching the  $S_1/S_0$  crossing.

Finally, we collected the  $S_1/S_0$  crossing configurations sampled from  $S_1$  AMD simulations, when the gap  $\Delta E_{S_0-1}$  becomes smaller than 0.1 eV. These AMD trajectories were continued on the ground-state  $S_0$  potential energy surface at 300 K (i.e., transitions to the ground state were enforced) with the excess of energy ( $\Delta E_{S_0-1}$ ) being dispersed in a nuclear kinetic energy. In this way, the photoproduct of COT is connected with the thermal reaction paths that include the  $S_0$  potential energy surface. As a comparison, pure thermal reaction channel simulations were also initiated on  $S_0$  from a ground-state optimized  $D_{2d}$  boat shape and planar  $D_{4h}$  COT structures, respectively. Figure 4b shows the time-dependent energy profiles of both  $D_{2d}$  and  $D_{4h}$  thermal reaction dynamics on  $S_0$ : it takes  $\sim 0.2$  ps for the system to reach the target temperature (300 K), then the plots demonstrate that the planar  $D_{4h}$  COT ultimately equilibrates to a  $D_{2d}$  boat-shaped structure by crossing an energy barrier. As shown in Figure 4c, the  $S_0$  AMD starting from the  $S_1/S_0$  conical intersection structure exhibits a coinciding equilibration progress as the

thermal reaction path of the planar  $D_{4h}$  structure, and the structure at the observed barrier from the thermal reaction MD is similar to the  $S_1/S_0$  crossing points where the excited-state branches of the MD are terminated. This establishes the connection between the  $S_1/S_0$  crossing structure and the continuous  $S_0$  simulations for a thermal reaction channel and, further, clarifies the final phase of COT in the ground-state dynamics toward an equilibrium boat-shaped geometry.

In summary, our dynamical simulations provide a comprehensive map of excited-state relaxation pathways in the photoexcited cyclooctatetraene. We used our NEXMD software to perform the nonadiabatic molecular dynamics simulation ( $S_{n>1}$  to  $S_1$  states) and adiabatic molecular dynamics simulation (at  $S_1$  and  $S_0$  states) of COT at ambient conditions. An active excited to ground-state relaxation pathway accompanied by a complete double-bond shifting progress of COT was determined as follows: boat-shaped  $D_{2d}$  structure ( $S_{n>1}$ )  $\rightarrow$  planar  $D_{8h}$  structure ( $S_1$ )  $\rightarrow$  slightly folded  $S_1$  metastable structure  $\rightarrow$  planar  $D_{4h}$  at  $S_1/S_0$  conical intersection  $\rightarrow$  boat-shaped  $D_{2d}$  ground-state equilibrium structure. Observed structural changes agree well with those determined from the high-level ab initio simulations. Moreover, the excitation lifetime obtained from our molecular dynamics simulation shows an excellent agreement with the experimental measurements. Our detailed dynamical results can thus provide a fundamental basis for further investigating the bond-order inversion and photoswitching process in the COT molecular systems.

## ■ ASSOCIATED CONTENT

### Supporting Information

The Supporting Information is available free of charge at <https://pubs.acs.org/doi/10.1021/acs.jpclett.1c01397>.

Potential energy analysis and geometric features analysis (PDF)

## ■ AUTHOR INFORMATION

### Corresponding Authors

Huajing Song – *Physics and Chemistry of Materials, Theoretical Division, Los Alamos National Laboratory, Los Alamos 87545, New Mexico, United States*; [orcid.org/0000-0001-5958-7377](https://orcid.org/0000-0001-5958-7377); Email: [songhw@lanl.gov](mailto:songhw@lanl.gov)

Sergei Tretiak – Physics and Chemistry of Materials, Theoretical Division and Center for Integrated Nanotechnologies, Los Alamos National Laboratory, Los Alamos 87545, New Mexico, United States; [orcid.org/0000-0001-5547-3647](https://orcid.org/0000-0001-5547-3647); Email: [serg@lanl.gov](mailto:serg@lanl.gov)

## Authors

Yeonsig Nam – Department of Chemistry, University of California, Irvine 92697, California, United States

Daniel Keefer – Department of Chemistry, University of California, Irvine 92697, California, United States

Marco Garavelli – Department of Industrial Chemistry, Università degli Studi di Bologna, Bologna 40136, Italy; [orcid.org/0000-0002-0796-289X](https://orcid.org/0000-0002-0796-289X)

Shaul Mukamel – Department of Chemistry, University of California, Irvine 92697, California, United States; Department of Physics and Astronomy, University of California, Irvine 92697, California, United States; [orcid.org/0000-0002-6015-3135](https://orcid.org/0000-0002-6015-3135)

Complete contact information is available at:

<https://pubs.acs.org/10.1021/acs.jpclett.1c01397>

## Notes

The authors declare no competing financial interest.

## ACKNOWLEDGMENTS

H.S., S.T., and S.M. acknowledge support from the U.S. Department of Energy (DOE), Office of Science, Basic Energy Sciences, Chemical Sciences, Geosciences, and Biosciences Division under Contract Nos. KC0301030 and KC030103172684 and Award No. DE-SC0019484. H.S. and S.T. acknowledge support of the Center for Integrated Nanotechnology at Los Alamos National Laboratory, a U.S. DOE and Office of Basic Energy Sciences User Facility. This research used resources provided by the LANL Institutional Computing Program. D.K. gratefully acknowledges support from the Alexander von Humboldt Foundation through the Feodor Lynen program.

## REFERENCES

- (1) Briquet, A. A. S.; Uebelhart, P.; Hansen, H.-J. Double-Bond Shifts in [4n]Annulenes as a New Principle for Molecular Switches: First Results with Dimethyl Heptalene-1,2- and -4,5-dicarboxylates. *Helv. Chim. Acta* **1996**, *79*, 2282–15.
- (2) Aprahamian, I. The Future of Molecular Machines. *ACS Cent. Sci.* **2020**, *6*, 347–358.
- (3) Zimmerman, H. E.; Iwamura, H. Thermal and photochemical interconversions of cyclooctatetraenes and semibullvalenes. Exploratory organic photochemistry. LII. *J. Am. Chem. Soc.* **1970**, *92*, 2015–22.
- (4) Sekkat, Z. In *Photoreactive Organic Thin Films*; Sekkat, Z., Knoll, W., Eds.; Academic Press: San Diego, CA, 2002; pp 271–287.
- (5) Neukirch, A. J.; Shamberger, L. C.; Abad, E.; Haycock, B. J.; Wang, H.; Ortega, J.; Prezhd, O. V.; Lewis, J. P. Nonadiabatic ensemble simulations of cis-stilbene and cis-azobenzene photoisomerization. *J. Chem. Theory Comput.* **2014**, *10*, 14–23.
- (6) Kandori, H.; Shichida, Y.; Yoshizawa, T. Photoisomerization in Rhodopsin. *Biochemistry (Moscow)* **2001**, *66*, 1197–1209.
- (7) Suomivuori, C.-M.; Gamiz-Hernandez, A. P.; Sundholm, D.; Kaila, V. R. I. Energetics and dynamics of a light-driven sodium-pumping rhodopsin. *Proc. Natl. Acad. Sci. U. S. A.* **2017**, *114*, 7043–48.
- (8) Garavelli, M.; Bernardi, F.; Cembran, A.; Castaño, O.; Frutos, L. M.; Merchán, M.; Olivucci, M. Cyclooctatetraene Computational

Photo- and Thermal Chemistry: A Reactivity Model for Conjugated Hydrocarbons. *J. Am. Chem. Soc.* **2002**, *124*, 13770–89.

(9) Garavelli, M.; Bernardi, F.; Moliner, V.; Olivucci, M. Intrinsically Competitive Photoinduced Polycyclization and Double-Bond Shift through a Boatlike Conical Intersection. *Angew. Chem., Int. Ed.* **2001**, *40*, 1466–68.

(10) Tokizaki, C.; Yoshida, T.; Takayanagi, T. Theoretical analyses of the time-resolved nuclear dynamics of the transition state for the 1,3,5,7-cyclooctatetraene unimolecular reaction. *Comput. Theor. Chem.* **2017**, *1112*, 20–26.

(11) Chang, J.-L.; Cheng, M.-Z.; Huang, Y.-J. Theoretical Study of the Negative Ion Photoelectron Spectrum of Cyclooctatetraene via Computation of Franck-Condon Factors. *J. Phys. Chem. A* **2020**, *124*, 3205–13.

(12) Yoshida, T.; Tokizaki, C.; Takayanagi, T. Theoretical analysis of the transition-state spectrum of the cyclooctatetraene unimolecular reaction: Three degree-of-freedom model calculations. *Chem. Phys. Lett.* **2015**, *634*, 134–139.

(13) Tokizaki, C.; Yoshida, T.; Takayanagi, T. Quantum Transition State Dynamics of the Cyclooctatetraene Unimolecular Reaction on Ab Initio Potential Energy Surfaces. *Chem. Phys.* **2016**, *469–470*, 97–104.

(14) Tully, J. C. Molecular Dynamics with Electronic Transitions. *J. Chem. Phys.* **1990**, *93*, 1061–1071.

(15) Nelson, T.; Fernandez-Alberti, S.; Roitberg, A.; Tretiak, S. Nonadiabatic excited-state molecular dynamics: Treatment of electronic decoherence. *J. Chem. Phys.* **2013**, *138*, 224111–224124.

(16) Fernandez-Alberti, S.; Roitberg, A. E.; Nelson, T.; Tretiak, S. Identification of unavoided crossings in nonadiabatic photoexcited dynamics involving multiple electronic states in polyatomic conjugated molecules. *J. Chem. Phys.* **2012**, *137*, 14512–14522.

(17) Nelson, T.; Fernandez-Alberti, S.; Chernyak, V.; Roitberg, A.; Tretiak, S. Nonadiabatic Excited-State Molecular Dynamics Modeling of Photoinduced Dynamics in Conjugated Molecules. *J. Phys. Chem. B* **2011**, *115*, 5402–5414.

(18) Nelson, T.; Fernandez-Alberti, S.; Roitberg, A.; Tretiak, S. Nonadiabatic Excited-State Molecular Dynamics: Modeling Photo-physics in Organic Conjugated Materials. *Acc. Chem. Res.* **2014**, *47*, 1155–1164.

(19) Malone, W.; Nebgen, B.; White, A.; Zhang, Y.; Song, H.; Bjorgaard, J.; Sifain, A.; Rodriguez-Hernandez, B.; Freixas, V.; Fernandez-Alberti, S.; Roitberg, E.; Nelson, R.; Tretiak, S. NEXMD Software Package for Nonadiabatic Excited State Molecular Dynamics Simulations. *J. Chem. Theory Comput.* **2020**, *16*, 5771–5783.

(20) Tretiak, S.; Zhang, W. M.; Chernyak, V.; Mukamel, S. Excitonic couplings and electronic coherence in bridged naphthalene dimers. *Proc. Natl. Acad. Sci. U. S. A.* **1999**, *96*, 13003–13008.

(21) Stewart, J. J. P. Optimization of Parameters for Semiempirical Methods IV: Extension of MNDO, AM1, and PM3 to More Main Group Elements. *J. Mol. Model.* **2004**, *10*, 155–64.

(22) Li, S. L.; Marenich, A. V.; Xu, X.; Truhlar, D. G. Configuration Interaction-Corrected Tamm–Dancoff Approximation: A Time-Dependent Density Functional Method with the Correct Dimensionality of Conical Intersections. *J. Phys. Chem. Lett.* **2014**, *5*, 322–328.

(23) Nelson, T. R.; White, A. J.; Bjorgaard, J. A.; Sifain, A. E.; Zhang, Y.; Nebgen, B.; Fernandez-Alberti, S.; Mozysky, D.; Roitberg, A. E.; Tretiak, S. Non-adiabatic Excited-State Molecular Dynamics: Theory and Applications for Modeling Photophysics in Extended Molecular Materials. *Chem. Rev.* **2020**, *120*, 2215–87.

(24) Zheng, F.; Fernandez-Alberti, S.; Tretiak, S.; Zhao, Y. Photoinduced Intra- and Intermolecular Energy Transfer in Chlorophyll a Dimer. *J. Phys. Chem. B* **2017**, *121*, 5331–39.

(25) Mukazhanova, A.; Malone, W.; Negrin-Yuvero, H.; Fernandez-Alberti, S.; Tretiak, S.; Sharifzadeh, S. Photoexcitation dynamics in perylene diimide dimers. *J. Chem. Phys.* **2020**, *153*, 244117.

(26) Stevenson, C. D.; Brown, E. C.; Hrovat, D. A.; Borden, W. T. Isotope Effects on the Ring Inversion of Cyclooctatetraene. *J. Am. Chem. Soc.* **1998**, *120*, 8864–67.

- (27) Paquette, L. A. The current view of dynamic change within cyclooctatetraenes. *Acc. Chem. Res.* **1993**, *26*, 57–62.
- (28) Nishinaga, T.; Ohmae, T.; Iyoda, M. Recent Studies on the Aromaticity and Antiaromaticity of Planar Cyclooctatetraene. *Symmetry* **2010**, *2*, 76–97.
- (29) Gellini, C.; Salvi, P. R. Structures of Annulenes and Model Annulene Systems in the Ground and Lowest Excited States. *Symmetry* **2010**, *2*, 1846–24.
- (30) Palmer, M. H.; Hoffmann, S. V.; Jones, N. C.; Coreno, M.; de Simone, M.; Grazioli, C. The electronically excited states of cyclooctatetraene—An analysis of the vacuum ultraviolet absorption spectrum by ab initio configuration interaction methods. *J. Chem. Phys.* **2019**, *151*, 084304.
- (31) Frueholz, R. P.; Kuppermann, A. Electronic spectroscopy of 1,3,5,7-cyclooctatetraene by low-energy, variable-angle electron impact. *J. Chem. Phys.* **1978**, *69*, 3614–21.
- (32) Kobayashi, Y.; Chang, K. F.; Poullain, S. M.; Scutelnic, V.; Zeng, T.; Neumark, D. M.; Leone, S. R. Coherent electronic-vibrational dynamics in deuterium bromide probed via attosecond transient-absorption spectroscopy. *Phys. Rev. A: At., Mol., Opt. Phys.* **2020**, *101*, 063414.
- (33) Parker, S.; Rappoport, D.; Furche, F. Quadratic Response Properties from TDDFT: Trials and Tribulations. *J. Chem. Theory Comput.* **2017**, *14*, 18999–19010.
- (34) Parker, S.; Roy, S.; Furche, F. Multistate hybrid time-dependent density functional theory with surface hopping accurately captures ultrafast thymine photodeactivation. *Phys. Chem. Chem. Phys.* **2019**, *21*, 18999–19010.
- (35) Stojanović, L.; Bai, S.; Nagesh, J.; Izmaylov, A. F.; Crespo-Otero, R.; Lischka, H.; Barbatti, M. New Insights into the State Trapping of UV-Excited Thymine. *Molecules* **2016**, *21*, 1603.
- (36) Szabo, A.; Ostlund, N. S. *Modern quantum chemistry: introduction to advanced electronic structure theory*; Courier Corporation, 2012.
- (37) Levine, B. G.; Ko, C.; Quenneville, J.; Martinez, T. J. Conical intersections and double excitations in time-dependent density functional theory. *Mol. Phys.* **2006**, *104*, 1039–1051.
- (38) Tapavicza, E.; Bellchambers, G. D.; Vincent, J. C.; Furche, F. *Ab Initio* non-adiabatic molecular dynamics. *Phys. Chem. Chem. Phys.* **2013**, *15*, 18336–18348.
- (39) Zhang, Y.; Mukamel, S.; Khalil, M.; Govind, N. Simulating Valence-to-Core X-ray Emission Spectroscopy of Transition Metal Complexes with Time-Dependent Density Functional Theory. *J. Chem. Theory Comput.* **2015**, *11*, 5804–5809.
- (40) Furche, F.; Perdew, J. P. The performance of semilocal and hybrid density functionals in 3d transition-metal chemistry. *J. Chem. Phys.* **2006**, *124*, 044103.
- (41) Fabiano, E.; Keal, T. W.; Thiel, W. Implementation of surface hopping molecular dynamics using semiempirical methods. *Chem. Phys.* **2008**, *349*, 334–437.
- (42) Song, H.; Fischer, S. A.; Zhang, Y.; Cramer, C. J.; Mukamel, S.; Govind, N.; Tretiak, S. First Principles Nonadiabatic Excited-State Molecular Dynamics in NWChem. *J. Chem. Theory Comput.* **2020**, *16*, 6418.
- (43) Savitzky, A. A.; Historic Collaboration. *Anal. Chem.* **1989**, *61*, 921A–23A.



# Non-adiabatic Molecular Dynamic Study of the Relaxation Pathways for Photoexcited Cyclooctatetraenes: Supporting Information

H. Song<sup>\*,†</sup>, Y. Nam<sup>‡</sup>, D. Keefer<sup>‡</sup>, M. Garavelli<sup>¶</sup>, S. Mukamel<sup>‡,§</sup>, and S. Tretiak<sup>\*,†,||</sup>

<sup>†</sup> *Physics and Chemistry of Materials, Theoretical Division, Los Alamos National Laboratory, Los Alamos, New Mexico, 87545, USA*

<sup>‡</sup> *Department of Chemistry, University of California, Irvine, CA 92697, USA*

<sup>¶</sup> *Department of Industrial Chemistry, "T. Montanari", Università degli Studi di Bologna, Viale del Risorgimento, 4, 40136 Bologna, Italy*

<sup>§</sup> *Department of Physics and Astronomy, University of California, Irvine, CA 92697, USA*

<sup>||</sup> *Center for Integrated Nanotechnologies, Los Alamos National Laboratory, Los Alamos, New Mexico 87545, USA*

*E-mail: songhw@lanl.gov; serg@lanl.gov*

## S1. Potential Energy Analysis

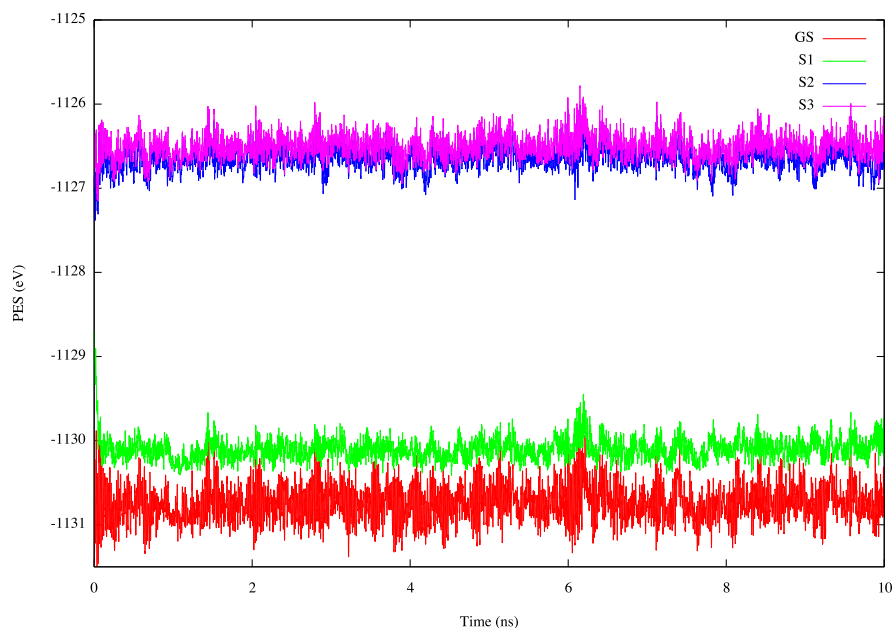


Fig S1. Ground to  $S_3$  potential energy profile of  $D_{8h}$  symmetric planar structure running in  $S_1$  AMD simulation.



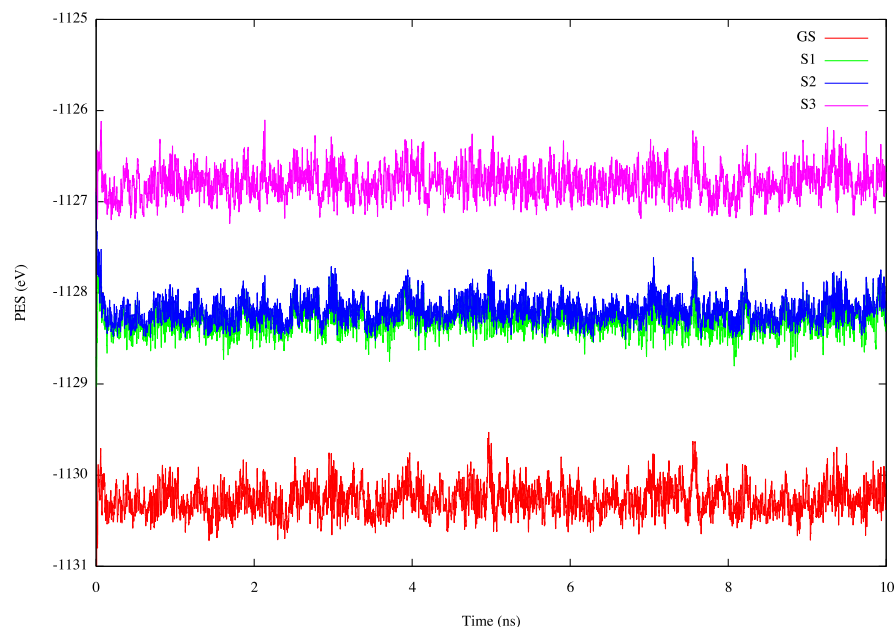


Fig S2. Ground to  $S_3$  potential energy profile of  $D_{2d}$  symmetric planar structure running in  $S_2$  AMD simulation.

According to the potential energy plots shown in Fig S1 and S2. The potential of  $S_2$  will be overlapped with  $S_3$  when the COT structured in a boat-shaped. On the other hand, the potential of  $S_2$  will be close to  $S_1$  when COT in a planar structure. It shows that there is no local minimum on  $S_2$  except the  $S_2/S_1$  conical intersection. Indeed, we unable to optimize the structure of COT in  $S_2$ .

## S2. Geometric Features Analysis

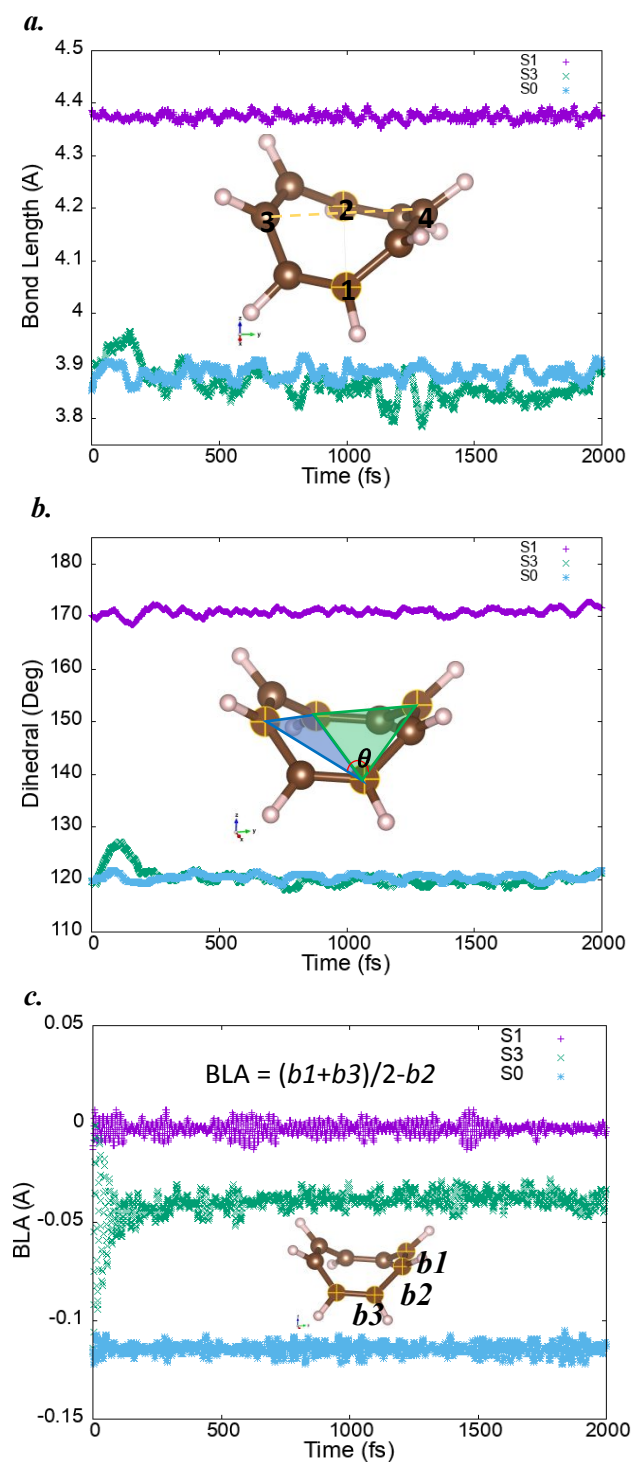


Fig S3. Geometric features analysis: (a.) Average Bond-Length, (b.) Dihedral Angles, and (c.) Bond Length Alternation (BLA). These 3 geometric features show significantly distinguishing between the planar and boat-shaped structure. Therefore, they are used to monitor the geometry evolution of COT during NAMD process.